IEEE Photonics Journal
An IEEE Photonics Society Publication

Intrusion Discrimination in Terms of LMD and ICA With Combined Features in The Fiber-Optic Perimeter System

Volume 12, Number 2, April 2020

Meng Li
Yifei Zhao
Yuzhao Ma
Guizhong Zhang

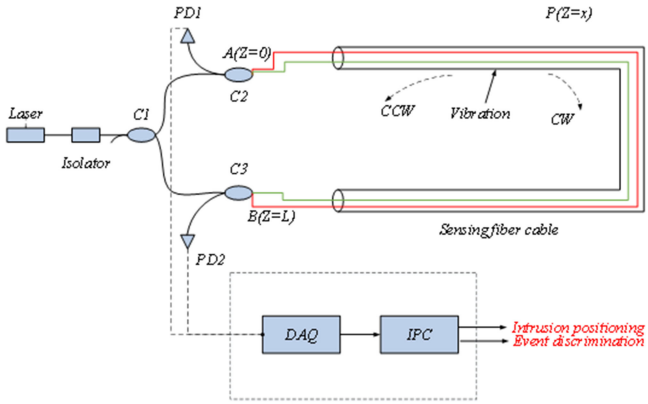

DOI: 10.1109/JPHOT.2020.2983011

Intrusion Discrimination in Terms of LMD and ICA With Combined Features in The Fiber-Optic Perimeter System

Meng Li,[1,2] **Yifei Zhao**,[1] **Yuzhao Ma**,[1] **and Guizhong Zhang**[2]

[1]Key Laboratory of Operation Programming, Safety Technology of Air Traffic Management, Civil Aviation University of China, Tianjin 300300, China.
[2]College of Precision Instrument and Optoelectronics Engineering, Tianjin University, Tianjin 300072, China.

DOI:10.1109/JPHOT.2020.2983011

Manuscript received January 20, 2020; revised March 6, 2020; accepted March 21, 2020. Date of publication March 30, 2020; date of current version April 14, 2020. Corresponding author: Meng Li (e-mail: 867750570@163.com.)

Abstract: For improving the performance of intrusion discrimination in the dual Mach-zehnder interferometric (DMZI) perimeter system, we propose a novel method based upon local mean decomposition (LMD), independent component analysis (ICA) and features combination. By the LMD-ICA, the original signal is processed to construct a virtual noise, thereby obtaining the sensitive information of the signal. With multiple features from the sensitive information, the type of intrusions can be discriminated by the method of serial feature fusion (SFF). The experiments are performed with real data for the case of the single-vibration and the single-vibration under the rain interference. The results demonstrate that the proposed method is superior to the traditional discrimination one, with an average recognition rate of over 96%.

Index Terms: Intrusion discrimination, local mean decomposition (LMD), independent component analysis (ICA), features combination.

1. Introduction

As a sophisticated phase-modulation fiber sensing technique, dual Mach-zehnder interferometric (DMZI) system [1], [2] possesses the superiority of fast response and high sensitivity, and has been extensively employed in the realms of pipeline leakage detection [3], submarine cable security [4], airport guarding [5], et al. For improving the efficiency of the DMZI system, several critical issues are proposed, involving endpoint detection [6], background noise removing [7], intrusion positioning [8], [9] as well as intrusion discrimination. Nevertheless, due to the diversity and complexity of invasion signals, feature description and classification for the intrusion signals are still immature. Especially for some complex environmental conditions, such as in an airport, the existing methods of feature discrimination can not reach high efficiency and high classification rate.

Therefore, in recent years, a series of investigations are carried out for improving the performance of intrusion discrimination. In 2015, Liu [10] proposed a combined method of intrusion discrimination based upon empirical mode decomposition, kurtosis characteristics and a radial basis function neural network. This method improves the average recognition rate to above 87%, which can meet actual requirements initially. In 2017, Huang [11] designed a novel intrusion discriminations scheme in terms of hybrid feature extraction for the DMZI system, which can identify

four common intrusions with an average rate of over 94%. In 2018, Ma [12] proposed intrusion discrimination for the DMZI sensing system, which applied the zero-crossing rate and multi-scale permutation entropy to complete intrusion features extraction, and calculate multiple event probabilities by a probabilistic support vector machine. This scheme can discriminate six common intrusions with an average recognition rate of over 92%. The essence of these existing methods is that decomposing the optical signal with advanced mathematical methods, and extracting the intrusion features in different scales. Therefore, the adaptability and capability of detail description for the decomposition method are the keys to improving the recognition rate of different intrusion events.

As an advanced time-frequency analysis method, local mean decomposition (LMD) [13]–[17] has been developed based on empirical mode decomposition (EMD) [18], [19], and can adaptively decompose a complex signal into the sum of product functions (PF) of several instantaneous frequencies. Compared with the classical EMD method, the LMD approach can suppress the endpoint effect [20], and eliminate the modal mixing effectively. However, when the vibration signal is affected by strong noise, the end effect and the false component still exist in the LMD, thus a certain approach is also necessary to extract the signal sensitive information from each component. For this purpose, the independent component analysis (ICA) [21]–[23] can be employed as a superior method to extract the intrinsic component in the aliased signal affected by strong noise, and separate different source signals from the aliased signal. However, as the second analysis of signal features based upon LMD, the ICA algorithm requires that the number of observation dimensions be greater than that of the source signals, which might cause the underdetermined problem for the case of insufficient observation dimensions. Additionally, vibration signals of different vibration types possess complex waveform features, which require more eigenvectors generated by ICA to reflect the features of the intrusion signal. Therefore, the optimized combination of multiple features is of significance to retain the effective information of intrusion signal, and eliminate the redundancy caused by the subjective and objective factors effectively.

In this paper, we propose a novel scheme of intrusion discrimination for the DMZI system, which is based on the LMD, ICA as well as serial feature fusion (SFF) [24]. With the LMD algorithm, the optical signal in the DMZI system is broken down into a series of PF, which is used as the ICA input to obtain the sensitive information of the intrusion signal. Then, four signal features, which are the zero-crossing rate [25], LMD energy entropy [26], the vibration signal kurtosis [27] and the approximate entropy [28], are employed to construct a feature entropy by the method of SFF. Finally, with the probabilistic neural network (PNN) [29], [30], different intrusion signals can be identified with high accuracy. Compared with existing methods that take the single feature into account, our method not only uses advanced LMD method to decompose the original signal, but also deploy multiple features to discriminate the vibration signal in terms of SFF, which can improve the adaptability of intrusion discrimination effectively. In the experiments, four kinds of vibration signals are used to test the proposed method with the real data.

2. Experimental Setup

The structure of DMZI vibration system is demonstrated in Fig. 1. The output of the laser is split equally by an isolator at coupler C1, and launched into the DMZI that involves coupler C2 and coupler C3. Then, two beams propagate in the clockwise(CW) and counter-clockwise(CCW), respectively, and interfere at C3 or C2. PIN diodes PD1 and PD2 can detect the interference outputs. The output signals of two PIN diodes are collected by data acquisition(DAQ) card. The detailed experimental parameters are shown in Table 1.

For testing the proposed method with real data, we fixed the DMZI system around one building in the way of sine shaped hanging. The length of the entire distributed fiber optic system is 2.5 km, with a laser source of 10 kHZ linewidth and 20 mW power. The sampling speed of the DAQ card is set to be 2 MSa/s, with 40000 sampling points generating after one vibration. The output intensity signal is:

$$I(t) = I_0 \exp\left(1 + K\cos\left(\Delta\varphi(t) + \varphi_0\right)\right) \tag{1}$$

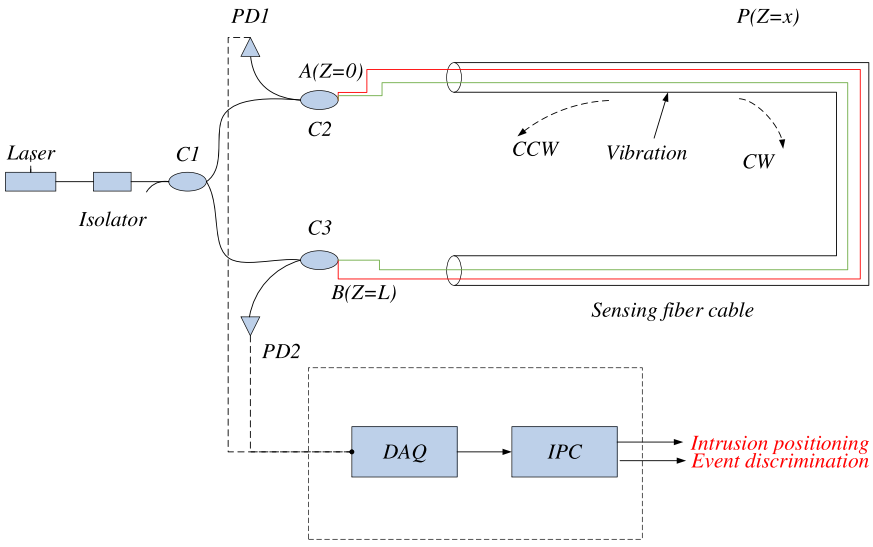

Fig. 1. Schematic diagram of DMZI intrusion sensor. DAQ: Data Acquisition; IPC: Industrial Personal Computer; C1, C2, C3: 3dB fiber coupler; and PD1, PD2: Photo-detector.

TABLE 1
Experiment Parameters

Experiment parameters	Value
Laser power	3.5mW
Laser wavelength	1550nm
Splitting ratio(C1,C2,C3)	50%
Length of two arms	2.5km
Media of the fiber	Sensing cable
Detector type	Photo-detector

where I_0 is the input of the laser light intensity; K is the visibility of the Mach-Zehnder interference; $\Delta\varphi(t)$ is the phase difference caused by external disturbance; φ_0 is the initial phase. Because it is difficult to extract phase information by phase demodulation, we use the time-frequency domain analysis method to calculate the change of the signal time-frequency parameter. Analyzing the output signal that contains the phase change of the light wave caused by the disturbance, we can identify the vibration type by the recognition algorithm. Wide frequency band, non-linear and non-stationary waveform, and lower signal to noise ratio are the characteristics of the optical signal in the DMZI system. Therefore, the LMD combined with the ICA algorithm is employed to extract sensitive information of the vibration signals.

3. Signal Reconstruction With the LMD and ICA

3.1 Local Mean Decomposition (LMD)

Local mean decomposition LMD is a novel non-stationary signal adaptive decomposition algorithm. After adaptively decomposing complex signals into a mixture of simple product functions (PF), the time-frequency distribution of the original signal can be obtained. The LMD process for the signal $x(t)$ is expressed as follows:

1) Determine all local extremum points of the original signal $x(t)$, termed as n_i. Calculate the mean value m_i of its adjacent extremum points and its envelope estimate a_i, which can be

expressed as:

$$\begin{cases} m_i = \frac{n_i + n_{i+1}}{2} \\ a_i = \frac{|n_i - n_{i+1}|}{2} \end{cases} \tag{2}$$

Connecting m_i and a_i with lines, and smoothing them by the moving average method, the local mean function $m_{11}(t)$ and local envelope estimation $a_{11}(t)$ can be obtained.

2) Separating m_{11}(t) from the original signal x(t), and one can obtain the residual signal h_{11}(t)

$$h_{11}(t) = x(t) - m_{11}(t) \tag{3}$$

3) Compute the frequency modulation function s_{11}(t)

$$s_{11}(t) = \frac{h_{11}(t)}{a_{11}(t)} \tag{4}$$

and repeat the above iterative process until the $(l+1)th$ local envelope estimation function $a_{1(l+1)}$ satisfies $a_{1(l+1)} = 1$.

4) Multiply all the local envelope estimation functions a_{11}, $a_{12}, \ldots, a_{1q}, \ldots, a_{1l}$, and obtain the instantaneous amplitude function:

$$a_1(t) = a_{11}(t)\, a_{12}(t) \cdots a_{1l}(t) = \prod_{q=1}^{l} a_{1q}(t) \tag{5}$$

5) Multiply the envelope signal a_1(t) by frequency modulation function s_{11}(t), and obtain the first PF component of the original signal.

$$P_1(t) = a_1(t)\, s_{1l}(t) \tag{6}$$

6) Separate the first PF component from the original signal x(t), and obtain a new signal u_1(t). Regard u_1(t) as the new original signal and repeat the above process k times until u_k(t) becomes a monotonic function.

7) Finally, the original signal x(t) can be decomposed into the sum of PF components and a monotonic function u_k(t):

$$x(t) = \sum_{i=1}^{k} P_i(t) + u_k(t) \tag{7}$$

3.2 The Combination Algorithm Based Upon LMD and ICA

The PF components extracted form original signal can be divided into the noise components and signal components. As the most effective method to evaluate the correlation between variables, the correlation coefficient can be used to distinguish the noise components from the signal components. In our view, the large correlation coefficient means a high correlation between the variables; and vice versa. Therefore, the PF components that have high correlation with the original signal can manifest more features of the original signal, and the ones that have low correlation with the original signal are regarded as the noise components. Alternatively, we apply t test to evaluate the significance of correlation coefficient between the PF component and original signal based upon statistics principles [31]. The steps of the significant test are shown in the following:

1) Calculate the correlation coefficient ρ_i for each PF components with the original signal by formula (8)

$$\rho_i = \frac{\sum_{j=1}^{R} \left(P_i(j) - \bar{P}_i(j)\right)\left(x(j) - \bar{x}(j)\right)}{\sum_{j=1}^{R} \left(P_i(j) - \bar{P}_i(j)\right)^2 \sum_{j=1}^{R} \left(x(j) - \bar{x}(j)\right)^2} \tag{8}$$

where R is the length of the signal, $P_i(j)$ and $x(j)$ are the discrete forms of the continuous signals $P_i(t)$ and $x(t)$, respectively.

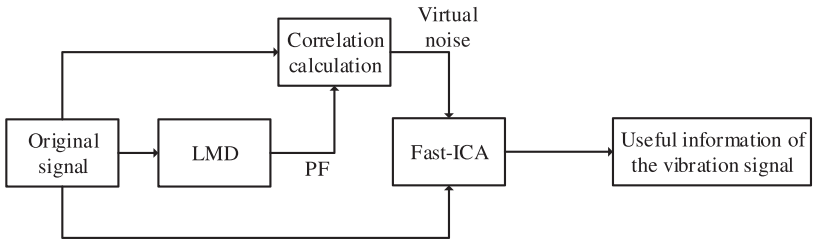

Fig. 2. Flow chart of signal reconstruction by the ICA and LMD.

2) The t test value of the correlation coefficient $\rho_i$can be expressed as:

$$t_i = \frac{\rho_i \sqrt{R-2}}{\sqrt{1-\rho_i^2}} \tag{9}$$

3) Based upon the given significance level α and freedom degrees (R-2), we can obtain the critical value in the t distribution table. When $|t_i| < t_{\alpha/2}$, ρ_i is considered as insignificant in statistics, thus the corresponding PF components make up virtual noise, termed as $N_0(t) = (N_1(t), N_2(t), \ldots, N_d(t))$

To extract the useful information of the original signal, we perform ICA with the original signal and virtual noise, as shown in Fig. 2. Based upon the high-order statistical features of the signal, ICA can separate the source signals from aliased multiple independent signals, thereby realizing the blind source separation of independent components in the signal. The mathematical model of the ICA algorithm is

$$\mathbf{X}(t) = \mathbf{A} \cdot \mathbf{S}(t) \tag{10}$$

where A is an unknown mixed matrix that superimposes the source signal, $\mathbf{S}(t) = [s_1(t), N(t)]^{\mathbf{T}}$, $s_1(t)$ and $N(t)$ are the signal components and noise components respectively in actuality. The essence of the ICA method is to estimate the $s_1(t)$ and $N(t)$ according to the observation signal $\mathbf{X}(t) = [x(t), N_1(t), N_2(t), \ldots, N_d(t)]^{\mathbf{T}}$. Note that in our method, the dimension of the observation signal $\mathbf{X}(t)$ is higher than that of the source signal $S(t)$ which is to be estimated, which satisfies the over-determination and ensures that the algorithm can accurately separate the components. Under the condition of unknown source signals and mixed matrix A, we calculate the optimal approximation of the source signal $S(t)$:

$$S'(t) = A^{-1} \cdot \mathbf{X}(t) \tag{11}$$

where $\mathbf{S}'(t) = [s_1'(t), N'(t)]^{\mathbf{T}}$, and $s_1'(t)$ is the estimation of useful information in the original vibration signal.

In different separation criteria, ICA algorithm can be expressed as many different algorithms. In our method, we select the fast ICA algorithm based on approximate maximum negative entropy [32] as a specific ICA method, which has a simple calculation with the characteristics of fast convergence and high robustness.

4. Feature Recognition With SFF-PNN

Feature based data fusion that generally combines multiple features into one integrated vector mainly involves two methods: one is the serial fusion, which forms the new vector based upon concatenating multiple independent ones, and can express the signal features in a higher-dimensional space; the other is parallel fusion, which translates multiple sets of features constitute into different complex vectors, and can reflect the signal features in the complex vector space. In this paper, as a simpler and easier way to fuse the signal features, the serial fusion is beneficial for the real-time processing of information, thereby selected as the method for data fusion.

To achieve accurate extraction and identification of the nonlinear characteristics of vibration signals, the characteristics of the time domain, frequency domain, energy distribution and complexity of the vibration signal are analyzed. The kurtosis, zero-crossing rate, LMD energy entropy and approximate entropy of the vibration signal are extracted to form an integrated feature vector by SFF. Finally, with the PNN in terms of learning classification, we can realize the recognition of different types of vibration signals.

4.1 Signal Features

4.1.1 Kurtosis: The kurtosis K is a dimensionless physical quantity that characterizes the time domain characteristics of the signal and is very sensitive to the external vibration in the DMZI system. If there is no external intrusion disturbance, the kurtosis of the signal is stable; if there is a vibration caused by the intrusion, the kurtosis value of the signal will increase. Different types of intrusions produce different shocks, resulting in different kurtosis values. Therefore, the kurtosis of the disturbance signal can be used to measure the time domain characteristics of different types of intrusion signals. According the references [33], [34], the expression of kurtosis can be expressed as:

$$K = \frac{1}{N}\sum_{j=1}^{N}\left(\frac{x_j - \bar{x}}{\sigma}\right)^4 \tag{12}$$

where N represents the length of the frame; x_j represents the jth signal ($j = 1 \sim$ N); $\bar{x}$ is the signal mean; σ indicates the signal standard deviation.

4.1.2 Short-Term Average Zero-Crossing Rate: The short-term average zero-crossing rate Z is a dimensionless physical quantity that characterizes the signal frequency. If there is no external intrusion disturbance, the short-term average zero-crossing rate of the signal is relatively low; if there is an external intrusion disturbance, a new frequency component is introduced, increasing the zero-crossing rate. Different types of disturbances introduce different frequency components, resulting in different zero-crossing rates of the signals. The general expression for the short-term average zero-crossing rate is

$$Z_r = \frac{1}{N}\sum_{j=1}^{N}\left|\operatorname{sgn}\{x[N\times(r-1)+j]\} - \operatorname{sgn}\{x[N\times(r-1)+j-1]\}\right| \tag{13}$$

where N represents the length of the frame; when $x > 0$, $\operatorname{sgn}\{x\} = 1$,when $x = 0$, $\operatorname{sgn}\{x\} = 0$. when $x < 0$, $\operatorname{sgn}\{x\} = -1$. r represents the number of frames; $x[N \times (r-1) + j]$represents the jth value in the rth frame of the signal ($j = 1 \sim$ N).

4.1.3 LMD Energy Entropy: The LMD energy entropy H is a dimensionless physical quantity that characterizes the uncertainty of signal energy distribution. If there is no external intrusion disturbance, the energy distribution of the signal is relatively stable, and the value of LMD energy entropy is relatively stable; if there is external intrusion disturbance, the signal energy distribution will change, and the corresponding energy entropy value will also change. LMD energy entropy is defined as

$$H = -\sum_{p=1}^{k} p_p \mathrm{lb}\, p_p \tag{14}$$

In Eq. (14), k is the number of PF components after LMD;$E_p = \|P_{PF}p\|^2$ indicates the energy of the pth PF component, $E = \|x\|^2$ is the total energy of the signal, $p_p = E_p/E$ represents the ratio of the signal energy of the pth PF component to the total energy of the signal.

4.1.4 Approximate Entropy: The approximate entropy E_{apen}(a,b) is a dimensionless physical quantity that characterizes the complexity of the signal. If there is no external intrusion disturbance, the signal is more regular and less complex, and the corresponding approximate entropy is smaller. If there is a disturbance, the disturbance increases the complexity of the signal, and

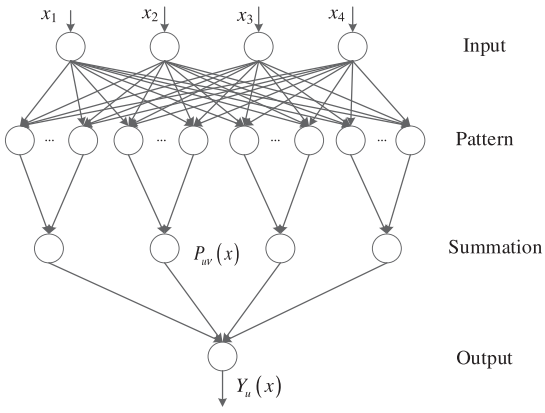

Fig. 3. Structural diagram of the PNN network.

the approximate entropy of the signal increases. Generally, the approximate entropy of model dimension value a = 2 and similar tolerance value b = 0.20STD (STD is the standard deviation of signal) is reasonable for feature extraction.

4.2 Serial Feature Fusion

Serial feature fusion combines multiple sets of feature components in a sample space into a new set of feature vectors. For the vibration signal of the optical fiber warning system, it is assumed that A_1, A_2, A_3, and A_4 are the above four characteristics in the model sample space respectively, and in any model sample, the kurtosis K$\in A_1$, the short-term average zero-crossing rate Z$\in A_2$, LMD energy entropy H$\in A_3$, approximate entropy Eapen$\in A_4$, the four features are serially combined to form a new set of integrated feature vectors, which can be expressed as:

$$\gamma = \left[K, Z, H, E_{\text{apen}}\right] \tag{15}$$

The integrated feature vector is considered as a classifier to perform learning classification, thereby breaking the limitation of classifying and identifying with a single feature.

4.3 Pattern Recognition

The probabilistic neural network(PNN) is a supervised classifier based on Bayesian minimum risk criteria, which belongs to a radial basis and forward feedback network. As shown in Fig. 3, the network structure is divided into four layers: input layer, model layer, summation layer, and output layer. Different from other common neural networks, the weights in the PNN are the training samples, thus the procedure of weight setting and revision can be omitted, which shortens the training time greatly. The steps of sample training and discrimination are demonstrated in the following:

1) Calculate the features of the training samples, and generate the feature vectors x_1, x_2, x_3, x_4. Pass the feature vectors to the pattern layer, and set them as the x_{uv}. μ indicates the type of training samples(claiming, knocking, car and wind), and νdenotes the sample number of one type.
2) Calculate the features of the test samples, termed as x. In the summation layer, for each feature, the similarity of the test samples and training samples are expressed as:

$$P_{\mu\nu}(x) = \frac{1}{M(2\pi)^{h/2}\omega^h} \exp\left[-\frac{(x - x_{uv})^{\mathrm{T}}(x - x_{uv})}{2\omega^2}\right] \tag{16}$$

TABLE 2
Four Types of Intrusion Actions

Intrusion actions	Experiments
Fence-climbing	Experimenter climb the fence. (160 samples)
Knocking	Experimenter knocked the defence. (157 samples)
Car	Experimenter drive the car near the fence. (155 samples)
Wind	The wind blows the fence 158 times. Note that 10 min is regarded as 1 sample.(158 samples)

where h is the dimension of feature vector, and $\omega$is the smoothing parameter that is assumed to be 1.

3) In the output layer, the feature vectors are summed to generate the probability function.

$$Y_\mu(x) = \sum_{v=1}^{M} P_{\mu v}(x) \tag{17}$$

Finally, the sample type corresponding the maximum of the probability function $Y_\mu(x)$ is the recognition result of the test samples.

5. Experimental Results and Discussions

5.1 Experiments for the Single Vibration

To verify the performance of the proposed method further, we carried out 630 trials including four types of intrusion actions, which are fence-climbing, knocking), car and wind, as shown in Table 2. 180 of them are used as PNN training data sets, and the others are applied as test sample sets. A sensing cable (2.5 kilometer long with single mode) was looped up and down and attached through hose clamps.

The effects of the method are verified by three common vibration modes and disturbance signals under natural wind conditions. The waveforms of the four typical disturbance signals collected in the field experiment are shown in Fig. 4. Fig 4(a) shows the vibration signal of the DMZI system when someone climbs the fence(completed by a 75 kg person); Fig. 4(b) shows the signal of the system output when the fence is knocked (completed by a 75 kg person); Fig. 4(c) shows the signal impacted by the roadside car (Peugeot 408, 2014); Fig. 4(d) displays the signal in the DMZI system disturbed by the natural wind (wind rating is 3∼4).

By LMD, the original signal is decomposed into a series of product functions that can be used to calculate the correlation coefficient with the original signal. As is stated above, If the PF components with large cross-correlation coefficients are summed for reconstructing the original signal, the irrelevant amounts caused by the noise or interference in each PF component are highly mixed, which may lead to an increase of unrelated quantities, thereby affecting the stability of the subsequent features extraction. However, for our method, a small number of the PF component with a smaller cross-correlation coefficient is used to reconstruct the virtual noise signal, which can reflect the characteristics of the noise to be separated in the original signal. In Fig. 5, we demonstrate the reconstructed knocking signal by LMD-ICA.

Four typical vibration signals are selected and processed using the proposed method and the corresponding four eigenvalues are calculated, as shown in Table 3. It can be seen that (1) the characteristic values of the knocking signal are the highest; (2) except for the kurtosis feature K, the eigenvalues of the natural wind signal are lower than the other three kinds of intrusions; (3)the approximate entropy of the climbing and natural wind signals is relatively close, but The kurtosis of the two are clearly differentiated;(4) similarly, the short-term average zero-crossing rate Z of

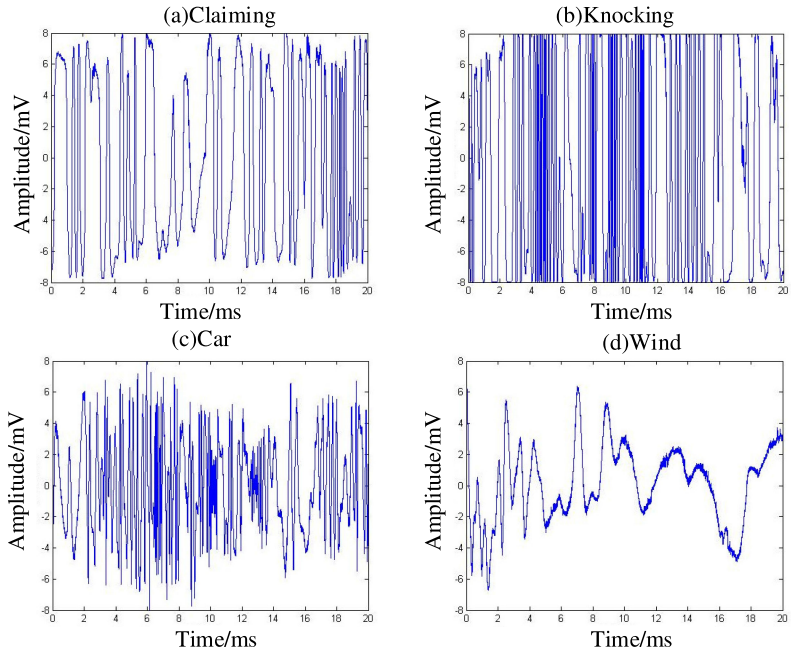

Fig. 4. The vibration signals of climbing (a), knocking (b), car (c), and wind (d).

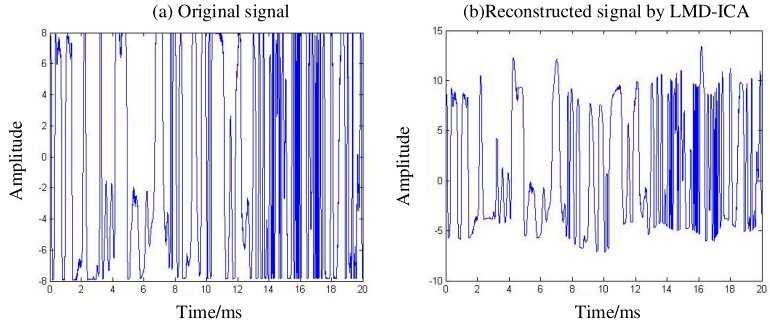

Fig. 5. Original signal (a) is processed to generate the reconstructed knocking signal by LMD- ICA (b).

the climbing and car signals are similar, but the other three features are clearly distinguished. Therefore, based upon the selected features we can distinguish different intrusions effectively, with lower feature dimensions.

For verifying the proposed method with real data, we select four groups of vibration signals that correspond to the vibration signals of car, knocking, climbing, and wind, respectively. Each group involves 10 samples that are employed to calculate the four feature values, as shown in Fig. 6. For the kurtosis, it is very sensitive to the instantaneous frequency in the signal, thus the impacts of knocking and climbing on the kurtosis of vibration signal are obvious, compared with the car and natural wind, as demonstrated in Fig. 6(a). In Fig. 6(b), the short-term average zero-crossing rate can reflect the allover frequency features of different disturbance signals, which can distinguish the vibrations between the knocking and the natural wind when the time-frequency distribution of their signals is similar. Since each PF component contains different frequency information, the LMD energy entropy can display the distribution feature of different vibration signals in the frequency domain. As shown in Fig. 6(c) the LMD energy entropy for knocking is the largest, and the one

TABLE 3
The Features Values of Four Types of The Vibration Signal

Intrusion	K	Z	H	E_{apen}
Climbing	1.69	94	1.98	0.0106
Knocking	1.80	258	2.59	0.1243
Car	1.21	115	2.33	0.0645
Wind	1.33	29	1.72	0.0078

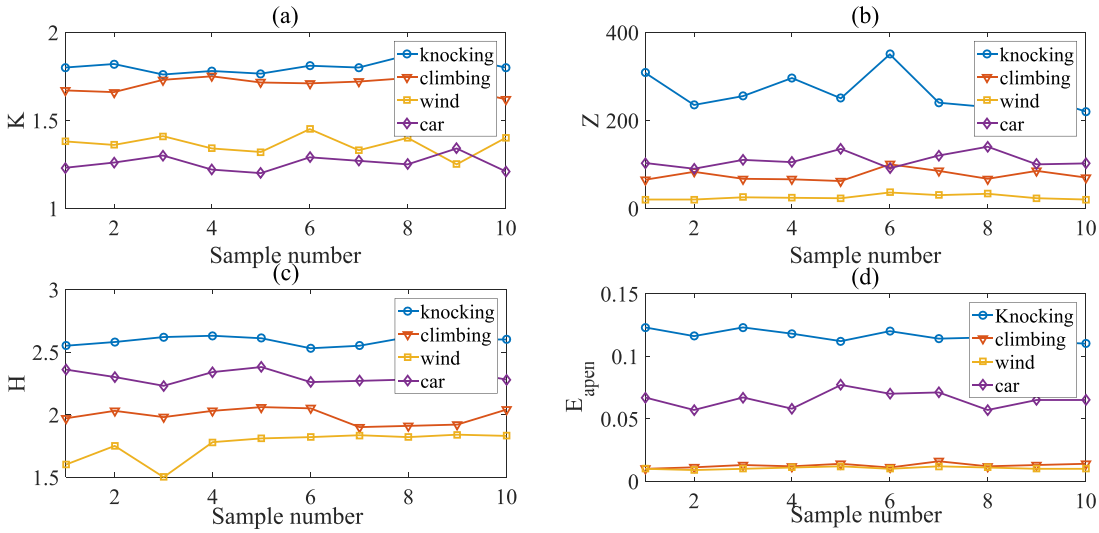

Fig. 6. Distributions of the Kurtosis (a), Short-term average zero-crossing rate (b), LMD energy entropy (c), and Approximate entropy (d) for different intrusion types.

for wind is the smallest. Different vibration signals have different time domain distributions, approximate entropy characteristics can be used to measure the complexity of time domain distribution of the vibration signal. Therefore, in Fig. 6(d), the approximate entropies of car and knocking are greater than climbing and natural wind.

In our method, multiple features are combined to discriminate the types of vibration signals, which can avoid the errors caused by the limitation of single feature discrimination. For example, in Fig. 6(a), only with the kurtosis, it is different to distinguish the car and wind, but if the other three features are considered, we can classify them easily. Similarly, the approximate entropy of the natural wind and climbing signal are relatively close, but other features such as the kurtosis can be used to supplement the description, so that the two types of vibration signals can be correctly identified.

TABLE 4
Recognition Results Based Upon Different Combined Features

Combined features	Climbing	Knocking	Car	Wind	Average recognition rate	Average recognition time/s
K,Z	65%	83%	61%	52%	65.3%	0.72
K,Z,H	95%	93%	88%	80%	89%	0.80
K,Z,H,E_{apen}	100%	100%	95%	92%	96.8%	0.87

TABLE 5
Recognition Results of Three Methods

method	Climbing	Knocking	Car	Wind	Average recognition rate	Average recognition time/s
Our method	100%	100%	94%	90%	96%	0.84
Direct signal extraction	97%	92%	81%	80%	87.5%	0.79
Hybrid feature extraction	100%	97%	88%	85%	92.5%	0.78

The combinations of feature values are set to be (k,z), (k,z,H) and(H,K,Z,E_{apen}). In Table 4, we demonstrate the recognition rate and recognition time(it includes feature extraction time, training time and test time) of the three combined features. It can be found that the number of combined features has a positive relationship with the recognition rate, and has a negative relationship with the recognition time. More features can improve the recognition accuracy, and make the cost of calculation increase. For the case of (H,K,Z,E_{apen}), the recognition rate approaches 100%, which illustrates the significance of the feature combination to the recognition accuracy. For evaluating the performance of the ICA-LMD, we directly extract the signal feature and then identify them with PNN. Additionally, the experiments based on the hybrid feature extraction method (see [11] for details) were also performed. For the two compared methods, we use the same samples as our proposed method. Therefore, the comparisons are fair for each method. As demonstrated in Table 5, our method is superior to the other methods for the average recognition rate. Especially for the case of weak intrusions, such as car and wind, the average recognition rates are improved obviously. Compared with direct signal extraction, the ICA-LMD has a better effect on the signal reconstruction. Meanwhile, for the recognition time, the computational costs of the two methods are close.

5.2 Experiments for the Single Vibration in the Rain

As a common weather phenomenon, the rain has the characteristics of long duration and uniform distribution. For verifying our method in the special weather environment condition, we carry out the experiments of climbing and knocking in the rain (rainfall is 10 $\sim$ 25 mm), the results of which are shown in Fig. 7. With our method, we can obtain four feature values of the vibration signals caused by the only rain, the climbing and knocking in the rain, as displayed in Table 6. It can be observed

TABLE 6
The Features of Vibration Signal in Rain

type	K	Z	H	E_{apen}
rain	1.34	6	0.69	0.0025
Climbing in rain	1.51	164	1.77	0.0088
Knocking in rain	1.69	207	1.85	0.0144

TABLE 7
Recognition Results of Three Methods

method	Rain	Climbing in rain	Knocking in rain	Average recognition rate	Average recognition time/s
Our method	100%	95%	95%	96.67%	0.93
Direct feature extraction	97%	86%	85%	89.3%	0.81
Hybrid feature extraction	100%	90%	88%	92.67%	0.75

that the feature values of the only rain is the smallest. Comparing the Table3 and 6, we can found that the characteristic values of the vibration signals, when climbing and knocking in the rainy weather, are different from that of a single disturbance. To verify the effectiveness of our method to distinguish different types of disturbances in the rainy weather, 550 trials are carried out, including three types of intrusion actions: rain(179 times), climbing in the rain(180 times), and knocking in the rain(191 times).160 of them were used as PNN training samples, and the remaining 390 were used as test samples. After performing the proposed method, direct feature extraction and the hybrid feature extraction method, the corresponding recognition rates and recognition times are shown in Table 7. We also use the same samples as our proposed method for the comparisons. Due to the processing process of LMD-ICA, the recognition time (0.93 s) of the proposed method is longer than the recognition time (0.75 s) of the hybrid feature extraction and Direct feature extraction(0.81 s), but still meets the good real-time performance. Under the strong interference of the rainy weather, our method can distinguish different types of intrusions effectively with a high average recognition rate of 96.67%, which outshines the results of the hybrid feature extraction method, illustrating that our method has excellent robustness against the strong interference of harsh weather.

6. Conclusion

Aiming at the vibration signal recognition problem of distributed optical fiber sensor, a vibration signal identification method combining LMD and SFF is proposed. The method is verified by a single vibration signal and its vibration signal mixed with wind and rainy weather. The average recognition rate can reach 96% and 96.67%, respectively, and the recognition time is 0.87 s and 0.91 s respectively. The results show that the method can effectively improve the recognition rate of vibration type while balancing the real-time performance, thus opening a door to the intrusion recognition of fiber-optic sensors in perimeter security systems. However, further experiments and

studies are needed to further improve the recognition rate and to identify more types of vibration signals simultaneously.

Acknowledgements

The authors acknowledge the financial support by “National Natural Science Foundation of China (No. U1833111)”, “Open fund of research institute of air traffic management, China (No. KGYJY2018002)” and “the Fundamental Research Funds for the Central Universities, China (No. 3122018D029)”.

References

[1] Q. Chen *et al.*, “An elimination method of polarization-induced phase shift and fading in dual Mach-Zehnder interferometry disturbance sensing system,” *J. Lightw. Technol.*, vol. 31, no. 19, pp. 3135–3141, Oct. 2013.
[2] Q. Sun, D. Liu, H. Liu, and P. Shum, “Distributed fiber-optic vibration sensor using a ring mach–Zehnder interferometer,” *Opt. Commun.*,vol. 281, no. 6, pp. 1538–1544, 2008.
[3] Y. Zhou, S. Jin, J. Zhang, and L. Sun, “Study on the distributed optical fiber sensing technology for pipeline leakage detection,” *J. Optoelectronics. Laser*, vol. 16, no. 8, pp. 935–938, 2005.
[4] S. Xie, M. Zhang, S. Lai, and Y. Liao, “Positioning method for dual Mach–Zehnder interferometric submarine cable security system,” *Proc. SPIE*, vol. 7677, pp. 76 770A-1–76 770A-4, Apr. 2010.
[5] L. Jiang and R. Yang, “Identification technique for the intrusion of airport enclosure based on double mach–zehnderinterferometer,” *J. Comput.*, vol. 7, no. 6, pp. 1453–1459, 2012.
[6] X. Huang, J. Yu, K. Liu, T. Liu, and Q. Chen, “Configurable filter-based endpoint detection in DMZI vibration system,” *IEEE Photon. Technol. Lett.*, vol. 26, no. 19, pp. 1956–1959, Oct. 2014.
[7] S. Xie, M. Zhang, Y. Li, and Y. Liao, “Positioning error reduction technique using spectrum reshaping for distributed fiber interferometric vibration sensor,” *J. Lightw. Technol.*, vol, 30, no. 22, pp. 3520–3524, Nov. 2012.
[8] S. Xie, Q. Zou, L. Wang, M. Zhang, Y. Li, and Y. Liao, “Positioning error prediction theory for dual Mach–Zehnder interferometric vibration sensor,” *J. Lightw. Technol.*, vol. 29, no. 3, pp. 362–368, Feb. 2011.
[9] C. Ma *et al.*, “Long-range distributed fiber vibration sensor using an asymmetric dual Mach–Zehnder interferometers,” *J. Lightw. Technol.*, vol. 34, no. 9, pp. 2235–2239, May 2016.
[10] K. Liu *et al.*, “A high-efficiency multiple events discrimination method in optical fiber perimeter security system,” *J. Lightw. Technol.*, vol. 33, no. 23, pp. 4885–4890, Dec. 1, 2015.
[11] X. Huang, H. Zhang, K. Liu, Y. Wang, C. Ma, and Q. Chen, “Hybrid feature extraction-based intrusion discrimination in optical fiber perimeter security system,” *IEEE Photon. J.*, vol. 9, no. 1, Feb. 2017, Art. no. 7800212.
[12] P. Ma, K. Liu, J. Jiang, Z. Li, P. Li, and T. Liu, “Probabilistic event discrimination algorithm for fiber optic perimeter security systems,” *J. Lightw. Technol.*, vol. 36, no. 1, pp. 2069–2075, Dec. 1, 2018.
[13] H. Liu and M. Han, “A fault diagnosis method based on local mean decomposition and multi-scale entropy for roller bearings,” *Mech. Mach.Theory*, vol. 75, pp. 67–78, May 2014.
[14] M. Han and J. Pan, “A fault diagnosis method combined with LMD, sample entropy and energy ratio for roller bearings,” *Measurement*, vol. 76, pp. 7–19, Dec. 2015.
[15] J. Sun, Q. Xiao, J. Wen, and Y. Zhang, “Natural gas pipeline leak aperture identification and location based on local mean decomposition analysis,” *Measurement*, vol. 79, pp. 147–157, Feb. 2016.
[16] Z. Liu, Z. He, W. Guo, and Z. Tang, “A hybrid fault diagnosis method based on second generation wavelet de-noising and local mean decomposition forrotating machinery,” *ISA Trans.*, vol. 61, pp. 211–220, Mar. 2016.
[17] J. S. Smith, “The local mean decomposition and its application to EEG perception data,” *J. Roy. Soc. Interface*, vol. 2, no. 5, pp. 443–454, 2005.
[18] N. E. Hang, Z. Shen, S. R. Long, and M. C. Wu, “The empirical mode decomposition and the Hilbert spectrum for nonlinear and non-stationary time series analysis,” *Proc. R. Soc. Lond. Ser. A Math. Phys. Eng. Sci.*, vol. 454, pp. 903–995, 1998.
[19] Z. Qin, H. Chen, and J. Chang, “Signal-to-noise ratio enhancement based on empirical mode decomposition in phase-sensitive optical time domain reflectometry systems,” *Sensors*, vol. 17, no. 8, 2017, Art. no. 1870.
[20] S. Xia and G. Zhou, “Endpoint effect suppression based on multipoint extension in bearing fault diagnosis,” *Int. J. Pattern Recognit. Artif. Intell.*, vol. 33, no. 92019, Art. no. 1950015.
[21] K. Cai, Z. Wang, G. Li, and D. He, “Harmonic separation from grid voltage using ensemble empirical-mode decomposition and independent component analysis,” *Int. Trans. Elect. Energy Syst.*, vol. 27, no. 2, 2017, Art. no. 2405.
[22] X. Li, W. Zhong, A. Alphones, C. Yu, and Z. Xu, “Channel equalization in optical OFDM systems using independent component analysis,” *J. Lightw. Technol.*, vol. 32, no. 18, pp. 3206–3214, Sep. 2014.
[23] Q. Zhang *et al.*, “Modulation- format- transparent IQ imbalance estimation of dual-polarization optical transmitter based on maximum likelihood independent component analysis,” *Opt. Express*, vol. 27, no. 13, pp. 18055–18068, 2019.
[24] J. Yang, J. Yang, D. Zhang, and J. Lu, “Feature fusion: Parallel strategy vs. serial strategy,” *Pattern Recognit.*, vol. 36, pp. 1369–1381, 2003.
[25] Q. Chen, T. Liu, K. Liu, J. Jiang, Z. Shen, and Z. Ding, “An improved positioning algorithm with high precision for dual Mach–Zehnder interferometry disturbance sensing system,” *J. Lightw. Technol.*, vol. 33, no. 10, pp. 1954–1960, May 2015.
[26] Y. Yang, D. Yu, and J. Cheng, “A roller bearing fault diagnosis method based on EMD energy entropy and ANN,” *J. Sound Vib.*, vol. 294, pp. 269–277, 2006.

[27] M. Demenikov, "Optimization of hybrid imaging systems based on maximization of kurtosis of the restored point spread function," *Opt. Lett.*, vol. 36, no. 24, pp. 4740–4742, 2011.
[28] J. M. Yentes, N. Hunt, K. K. Schmid, J. P. Kaipust, D. McGrath, and N. Stergiou, "The appropriate use of approximate entropy and sample entropy with short data sets," *Annals Biomed. Eng.*, vol. 41, no. 2, pp. 349–365, 2013.
[29] T. Song, M. M. Jamshidi, R. R. Lee, and M. X. Huang, "A modified probabilistic neural network for partial volume segmentation in brain MR image," *IEEE Trans. Neural Netw.*, vol. 18, no. 5, pp. 1424–1432, Sep. 2007.
[30] T. A. Eriksson, H. Bulow, and A. Leven, "Applying neural networks in optical communication systems: Possible pitfalls," *IEEE Photon. Technol. Lett.*, vol. 29, no. 23, pp. 2091–2094, Dec. 2017.
[31] S. You and Y. Yu, *Statistics*. Wuhan, China: Wuhan Univ. Press, 2001, pp. 115–118.
[32] C. Rascon, B. Lennox, and O. Marjanovic, "Recovering independent components from shifted data using fast independent component analysis and swarm intelligence," *Appl. Spectrosc.*, vol. 63, no. 10, pp. 1142–1151, 2009.
[33] G. L. McDonald, Q. Zhao, and M. J. Zuo, "Maximum correlated Kurtosis deconvolution and application on gear tooth chip fault detection," *Mech. Syst. Signal Pr.*, vol. 33, pp. 237–255, 2012.
[34] S. Chong, G. Yang, and Y. Chen, "Blind extraction of nonstationary signal with four order correlation kurtosis deconvolution," in *Proc. Eur. Modelling Symp.*, 2016, pp.75–78.
[35] M. Kusy and R. Zajdel, "Application of reinforcement learning algorithms for the adaptive computation of the smoothing parameter for probabilistic neural network," *IEEE Trans. Neural Netw. Learning Syst.*, vol. 26, no. 9, pp. 2163–2175, Sep. 2015.